Macromolecules

pubs.acs.org/Macromolecules Article

# Methyl-Branched Side Chains on Polythiophene Suppress Chain Mobility and Crystallization to Enhance Photovoltaic Performance

Jia-Yi Chu, Chia-Yi Lin, Tsung-Han Tu, Shao-Huan Hong, Ya-Ying Chang, Chia-Wei Yang, Yi-Tsu Chan, Cheng-Liang Liu, Pavel V. Komarov, and Shih-Huang Tung*

Cite This: *Macromolecules* 2021, 54, 3689−3699 Read Online

ACCESS | Metrics & More | Article Recommendations | Supporting Information

**ABSTRACT:** We synthesized a polythiophene with methyl-branched side chains, poly(3-2-methylpentylthiophene) (P3MPT), and studied the thermal properties, morphology, optoelectrical properties, and photovoltaic performance of P3MPT blended with the fullerene derivative, [6,6]-phenyl $C_{60}$-butyric acid methyl ester (PCBM). The results are compared to those of the commonly used poly(3-hexylthiopene) (P3HT) with linear side chains to investigate the effects of the methyl-branched side chain. Differential scanning calorimetry (DSC) shows a higher glass transition temperature, and both X-ray diffraction and UV−vis absorption reveal a lower crystallization rate for P3MPT as compared to P3HT, due to the methyl-branched side chains that more efficiently suppress the chain mobility. Such behaviors can create an optimal as well as a stable structure for bulk-heterojunction solar cells so that the P3MPT/PCBM-based device not only shows a higher power conversion efficiency (PCE) but can much more effectively maintain the efficiency with time than the P3HT/PCBM-based device does. The stable phase-separated structure in the P3MPT/PCBM blend is confirmed by the grazing-incidence small-angle X-ray scattering (GISAXS) technique, which explains the superior long-term stability of the P3MPT/PCBM solar cell.

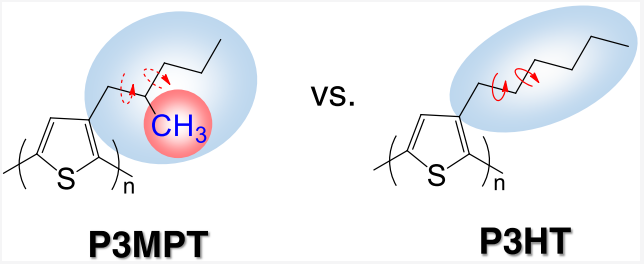


## INTRODUCTION

Poly(3-alkylthiophene)s (P3ATs) have been the most widely studied conjugated polymer because of their simple molecular structures and competent optoelectrical properties.[1] It has been known that the length of the alkyl side chain on P3ATs significantly influences the charge carrier transport and photovoltaic properties,[2,3] and P3HT with linear six-carbon side chains shows a superior photovoltaic performance among P3ATs.[4−6] In addition to P3ATs with linear alkyl side chains, the molecular packing and optical properties of P3ATs with branched alkyl side chains have been investigated,[7−10] and some reports have shown that the power conversion efficiency (PCE) of such P3ATs is comparable or lower than that of P3HT.[11,12] However, much less attention has been paid to the fundamental physical properties of P3ATs with branched alkyl side chains, such as the thermal properties and crystallization behaviors that in fact highly correlate with the photovoltaic performance. Particularly, the effect of the short branch, i.e., a methyl group, that can rigidify the side chain has not been systematically studied.

The most efficient polymer solar cells so far are based on the bulk-heterojunction structure of donor conjugated polymers blended with acceptor small molecules, mostly fullerene derivatives such as [6,6]-phenyl $C_{60}$-butyric acid methyl ester (PCBM), in active layers.[13−15] The success of bulk-heterojunction structure roots in the formation of the phase-separated bicontinuous donor and acceptor domains on a fine scale of ∼10 nm, which facilitate charge carrier separation at the widely accessible interfaces, as well as the transport of holes and electrons to electrodes through continuous pathways.[16−19] Previous reports have shown that some crystallinity is necessary both in the donor and acceptor domains for the charge carriers to transport efficiently.[20,21] However, over-crystallization can induce a large-scale phase separation that reduces the donor−acceptor interfaces and thus deteriorates the photovoltaic performance.[22−24] In addition, recent studies have suggested that a molecularly intermixed amorphous phase of the donor and acceptor is also crucial to the photovoltaic performance because the side-by-side packing between the donor and acceptor can promote a much faster charge separation process.[25−28] To achieve polymer solar cells with high photovoltaic performance and long-term stability, therefore, a balance between the crystalline and amorphous phases to create an optimal bulk-heterojunction structure that does not evolve with time is required. In this regard, the mobility of

Received: February 13, 2021
Revised: March 29, 2021
Published: April 12, 2021

Downloaded via SYNCHROTRON RADIATION RESEARCH on February 16, 2022 at 06:51:36 (UTC).
See https://pubs.acs.org/sharingguidelines for options on how to legitimately share published articles.

ACS Publications © 2021 American Chemical Society



https://doi.org/10.1021/acs.macromol.1c00346
*Macromolecules* 2021, 54, 3689−3699

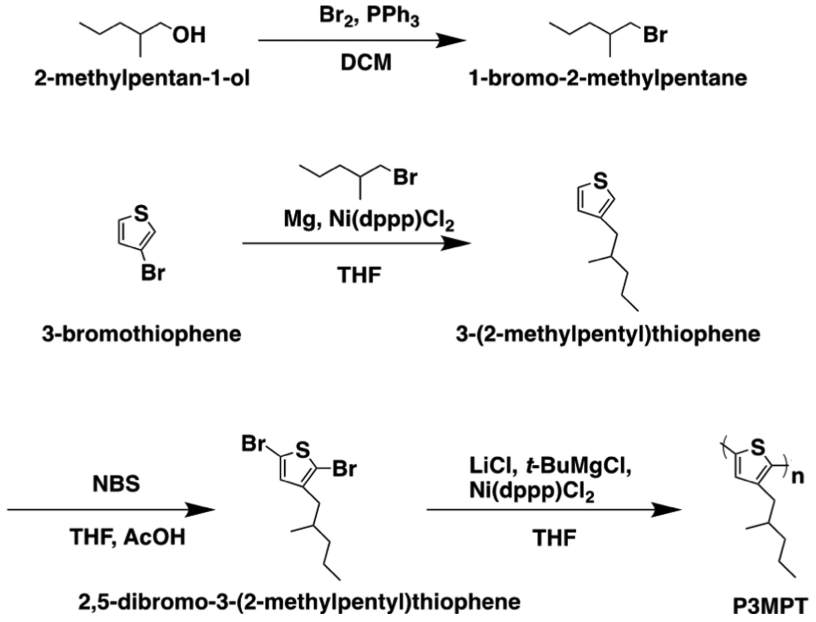


**Figure 1.** Synthesis route of P3MPT.

the polymer chain plays an important role because chain mobility is a major factor that controls the crystallization rate and the stability of the structure.

It is well known that the nature of the side group has a profound effect on chain mobility and affects the glass transition temperature $T_g$ (or the flexibility) of polymers. Bulkier side groups tend to cause a greater stiffening (higher $T_g$) through a restriction of bond rotation.[29] In this work, we synthesized a P3HT isomer, poly(3-2-methylpentylthiophene) (P3MPT), bearing methyl-branched side chains (Figure 1) instead of linear ones, and compared its properties and structures with those of P3HT. Such a short branch on side chains brings about the following effects. First, the methyl group on the side chain restricts the rotation of the adjacent C−C bonds, and thus the branched side chain is more rigid in comparison to the linear one on P3HT. This effect is absent for the branches longer than two carbons because they instead work as a spacer that softens the side chains.[30] Second, the methyl-branched side chains on P3MPT are bulkier than the linear side chains on P3HT such that the P3MPT backbone is less flexible than the P3HT backbone due to a severer hindered rotation, and also the packing of P3MPT cannot be as close as that of P3HT. It is thus expected that the chain mobility and the crystallization rate of P3MPT are lower than those of P3HT. Differential scanning calorimetry (DSC), X-ray diffraction, and UV−vis absorption techniques were used to confirm these arguments in this work.

Although amorphous P3ATs and PCBM are miscible,[31,32] the crystallization of P3ATs rejects PCBM out of the growing crystals and causes a crystallization-induced phase separation. Such a phase separation aggravates with time as the crystallinity of P3ATs increases, and the aggregates may grow to a scale larger than the exciton diffusion length so that the efficiency decreases accordingly.[16,31,32] Many efforts have been made to retard the phase separation in polymer/fullerene blends so as to enhance the stability of devices, including both the chemical[33−37] and physical methods.[38−41] In this work, we show that the suppressed chain mobility and crystallization of P3MPT have a positive effect on the photovoltaic performance of the P3MPT/PCBM devices, both on the PCE value and long-term stability. The slowdown of the chain motion and crystallization caused by the methyl-branched side chains decreases the crystallization-induced phase-separation rate between P3MPT and PCBM that is generally considered as a key factor responsible for the decay of polymer solar cells. This stable phase-separated structure for the P3MPT/PCBM blends is verified by the grazing-incidence small-angle X-ray scattering (GISAXS) technique.

## EXPERIMENTAL SECTION

**Materials.** The synthesis route of P3MPT is shown in Figure 1. The synthesis details and the characterization are described in the Supporting Information. The number-average molecular weight ($M_n$) of P3MPT is 16.5 kg/mol and the polydispersity index (PDI) is 1.30. P3HT was purchased from 1-Material. The $M_n$, PDI, and regioregularity are 50.0 kg/mol, 1.52, and >95%, respectively. The gel permeation chromatograms (GPCs) of P3MPT and P3HT are shown in Figure S6. PCBM with purity >99.5% was purchased from 1-Material. The chemicals were used as received.

**Device Fabrication.** The solar cell devices were fabricated with an inverted architecture with indium/tin oxide (ITO) glass as the cathode and Ag as the anode. For the preparation of zinc oxide (ZnO) thin film, 0.88 g of $Zn(CH_3COO)_2{\cdot}2H_2O$ was dissolved in 5 mL of 2-methoxyethanol, which was then mixed with 0.275 mL of ethanolamine diluted in 5 mL of 2-methoxyethanol as the stabilizing agent. The solution was spin-coated on the ITO glass substrate with a thickness of ∼35 nm and then baked at 170 °C for 16 min in an oven. To prepare the active layers with better performance, P3MPT/PCBM blends were dissolved in 1,2,4-trichlorobenzene (TCB) while P3HT/PCBM blends were dissolved in 1,2-dichlorobenzene (ODCB). The concentrations of P3MPT and P3HT were 20 and 15 mg/mL, respectively. The solutions were stirred at 60 °C for more than 72 h to ensure complete dissolution, then cooled to room temperature. The active layers were then spin-coated from the solutions in a nitrogen-filled glovebox. The wet films were covered by Petri dishes and slowly dried for 16 h. The thickness of the P3MPT/PCBM active layers was about 100 nm and that of the P3HT/PCBM active layer was about 130 nm. A 3.5 nm thick hole-transport molybdenum trioxide ($MoO_3$) layer and an ∼85 nm Ag electrode were then subsequently deposited via thermal evaporation. The completed devices were stored in a glovebox and covered by aluminum foil to prevent oxygen and light.


https://doi.org/10.1021/acs.macromol.1c00346
Macromolecules 2021, 54, 3689−3699

The current density versus voltage ($J$–$V$) curves were measured in ambient conditions using a Keithley 2400 source measurement unit under AM 1.5 G 100 mW/cm$^2$ illumination from an Oriel Sol13A solar simulator. For the space-charge-limited current (SCLC) measurements, the structure of the devices was similar to that of the solar cells except that the $MoO_3$ layer was replaced by a 20 nm thermal-evaporated $C_{60}$ layer in the electron-only devices and the ZnO layer was replaced by a 20 nm spin-coated $NiO_x$ layer in the hole-only devices. $NiO_x$ solution was prepared by dissolving nickel(II) 2,4-pentanedionate in 1 mL of ethanol containing HCl (36.5–38.0%, 10 $\mu$L) at a concentration of 0.1 M. The measurements were carried out on a Keithley 4200-SCS parameter analyzer at room temperature.

**Characterization.** The chemical structures of the synthesized compounds were characterized by $^1$H NMR spectroscopy performed on a Bruker 400 spectrometer, using *d*-chloroform as the solvent. Thermogravimetric analysis (TGA) was carried out on a TA Instruments Q50 in a nitrogen atmosphere. DSC thermograms were collected on a TA Instruments DSC 25 under a nitrogen atmosphere at a heating rate of 10 °C/min. Atomic force microscopy (AFM) images were taken under ambient conditions in tapping mode on a MultiMode AFM system with a Nanoscope three-dimensional (3D) controller (Digital Instruments/Veeco Metrology). Silicon cantilevers (PPP-NCHR-50 from Nanosensor) were used. Absorption spectra of the solutions and thin films were characterized using a Dynamica DB-20 UV–vis spectrometer in the range of wavelength from 300 to 800 nm. Thin-film samples were spin-coated on cleaned quartz substrates. Steady-state photoluminescence (PL) and time-resolved photoluminescence (TRPL) were recorded using an FLS980 fluorescence spectrometer (Edinburgh Instruments). Cyclic voltammetry measurements were carried out on a CH Instruments 621B electrochemical analyzer. The polymer solutions were dropped on a glassy carbon electrode to form films. Tetrabutylammonium hexafluorophosphate (TBAPF6) was added as an electrolyte, and 0.1 M ferrocene was used as an internal or external standard. The working, counter, and reference electrodes were glassy carbon, platinum wire, and Ag/$AgNO_3$, respectively. The external quantum efficiency (EQE) was measured using a QEX10 system (PV Measurements). Grazing-incidence small-angle and wide-angle X-ray scattering (GISAXS and GIWAXS) for thin films were carried out on beamline B23A1 in the National Synchrotron Radiation Research Center (NSRRC), Taiwan.[42] The wavelength $\lambda$ was 1.24 Å, and the incident angle was 0.2°. Thin films were spin-coated on a 1.5 cm × 1.5 cm silicon wafer.

**GISAXS Modeling.** We assume that the crystallites of polymers are polydisperse spherical particles and phase separation occurs between the polymer and PCBM. We thus combine the model of the polydisperse spherical particles[43] $I^S$ and the Debye–Anderson–Brumberger (DAB) model[44] $I^{DAB}$, which is commonly used for randomly distributed two-phase systems, i.e., $I(q) = I^S(q) + I^{DAB}(q)$, to fit the GISAXS profiles. The modeling was conducted using the package provided by NIST with IGOR Pro software.[45] The scattering function $I^S$ is given by

$$I^S(q) = (\Delta\rho)^2\left(\frac{4}{3}\pi\right)^2 \int_0^\infty f(R)R^6F^2(qR)\mathrm{d}R \quad (1)$$

Here, $\Delta\rho$ is the scattering contrast and $R$ is the radius of the particle. $F(qR)$ is given by

$$F(qR) = \frac{3[\sin(qR) - qR\cos(qR)]}{(qR)^3} \quad (2)$$

The distribution of the radius $f(R)$ is described by the Schulz equation[46]

$$f(R) = \left(\frac{z+1}{R_0}\right)^{z+1}\frac{R^z}{\Gamma(z+1)}\exp\left(-(z+1)\frac{R}{R_0}\right) \quad (3)$$

$R_0$ is the average radius and $\Gamma$ is $\gamma$ function. The polydispersity $p$ is given by

$$p = \frac{1}{\sqrt{z+1}} \quad (4)$$

The scattering function $I^{DAB}$ is given by

$$I^{DAB}(q) = \frac{A\xi^3}{[1+(q\xi)^2]^2} \quad (5)$$

Factor $A$ is an independent fitting parameter. $\xi$ is the correlation length, and a larger $\xi$ indicates a greater phase-separation scale.

## RESULTS AND DISCUSSION

**Thermal Properties and Structures.** The DSC heating thermograms of P3HT, P3MPT, and their blends with PCBM at a 1:1 weight ratio after quenching in liquid nitrogen are compared in Figure 2. The glass transition of P3HT

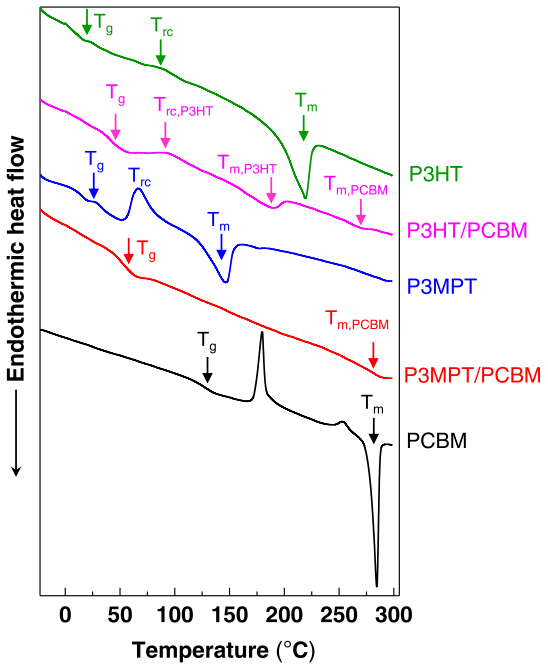


**Figure 2.** DSC heating thermograms of P3HT, P3MPT, and their blends with PCBM at a 1:1 weight ratio after quenching in liquid nitrogen.

indistinctly lies in the range between 0 and 30 °C, approximate to the reported $T_g$ of P3HT at 12 °C,[47] and that of P3MPT is more clearly seen between 10 and 40 °C. P3MPT shows a pronounced recrystallization $T_{rc}$ at 67 °C, and the crystal melts at 147 °C. The heat of recrystallization and the heat of melting are comparable, indicating that the crystallization is nearly suppressed during the quenching process. P3HT is still highly crystalline even under such a rapid cooling rate, judging from the small recrystallization at 89 °C and the large melting peak at 219 °C. The DSC data of the pristine polymers show that P3MPT exhibits a higher $T_g$, a lower crystallization rate, and a lower $T_m$ than P3HT. The architecture of the side chain has to play a key role in the thermal properties. The glass transition and crystallization rate of polymers are highly dependent on chain mobility. It is well known that the short methyl side groups retard the rotation of the single bonds on the chain and lower the chain mobility. The mobility of the methyl-branched side chains on P3MPT is therefore lower than the linear side chains on P3HT, which explains why P3MPT shows a higher $T_g$ and a lower crystallization rate. Furthermore, the methyl


https://doi.org/10.1021/acs.macromol.1c00346
Macromolecules 2021, 54, 3689–3699

side group disrupts the chain regularity, thus hindering the close packing of the side chains, and, also, the backbone packing is restricted by the bulkier methyl-branched side chains, both of which contribute to the lower $T_m$ of P3MPT.

The $T_g$ and $T_m$ of pure PCBM are 127 and 284 °C, respectively. After mixing with PCBM at a 1:1 weight ratio, the P3MPT/PCBM blend shows a clear $T_g$ at 54 °C. First, the single glass transition between pure P3MPT and PCBM implies that the amorphous P3MPT and PCBM are miscible, similar to the P3HT/PCBM blend reported previously.[31] Second, we can see that the $T_g$ of P3MPT/PCBM is higher than that of P3HT/PCBM (43 °C) at the same ratio, again implying slower chain mobility of P3MPT. Different from the P3HT recrystallization peak observed at 93 °C that is followed by a P3HT melting peak at 189 °C, the absence of the recrystallization and melting of P3MPT in the blend suggests that the incorporation of PCBM can nearly suppress the crystallization of P3MPT during the cooling and heating processes due to its slower crystallization rate. In other words, there is a greater fraction of miscible amorphous phase in the P3MPT/PCBM blend in comparison to the P3HT/PCBM one. Both blends show small exothermic peaks at around 280 °C, which corresponds to the melting of PCBM. The DSC data of the P3MPT/PCBM blend at varying weight ratios are shown in Figure S8 where we can see that the crystallization of P3MPT is suppressed as the PCBM content increases to the 1:0.6 weight ratio and the single $T_g$ is increased with increasing PCBM fraction, further evidencing good miscibility between amorphous P3MPT and PCBM.

Figure S9 shows the GIWAXS data of P3HT and P3MPT films spin-coated on a silicon wafer. Strong diffraction appears at $q_z$ = 0.42 Å$^{-1}$ with high-order peaks for P3HT while only the primary peak appears at $q_z$ = 0.47 Å$^{-1}$ for P3MPT. Both polymers arrange in an edge-on manner with interlamellar $d$-spacings of 15.0 and 13.4 Å, respectively. The smaller $d$-spacing of P3MPT is due to its shorter side chains. The weaker diffraction intensity of P3MPT indicates a lower crystallinity in comparison to P3HT in the as-cast film, which is consistent with the results of the DSC thermograms. The morphologies probed by AFM for the P3HT and P3MPT films drop-coated from dilute polymer solutions (0.05 mg/mL) onto silicon wafers are shown in Figure 3. P3HT forms locally aligned bundlelike fibers, whereas P3MPT forms randomly oriented fibers crossing one another. The methyl-branched side chain on polythiophene not only affects the molecular packing but also the macroscopic morphology of the aggregates. The AFM images of the blends are shown in Figure S10. The root mean square roughness $R_{ms}$ of the P3HT/PCBM and P3MPT/PCBM films are 5.54 and 9.98, respectively.

**Optical and Electrochemical Properties.** The normalized UV−vis absorption spectra of P3HT and P3MPT in solutions and as-cast thin films are compared in Figure 4a. The solvents for P3HT and P3MPT are ODCB and TCB, respectively, consistent with the solvents used in the device fabrication. In solutions, the absorption band of P3MPT (456 nm) is slightly lower than that of P3HT (459 nm). This is possibly because the branched side chain of P3MPT causes a larger steric hindrance for reaching a coplanar backbone than the linear one of P3HT does, thus resulting in a shorter conjugation length for P3MPT. The whole absorption spectra of the as-cast thin films are red-shifted from those of the solutions. P3MPT shows only a primary band at 506 nm, which is attributed to the intrachain absorption of the chains in

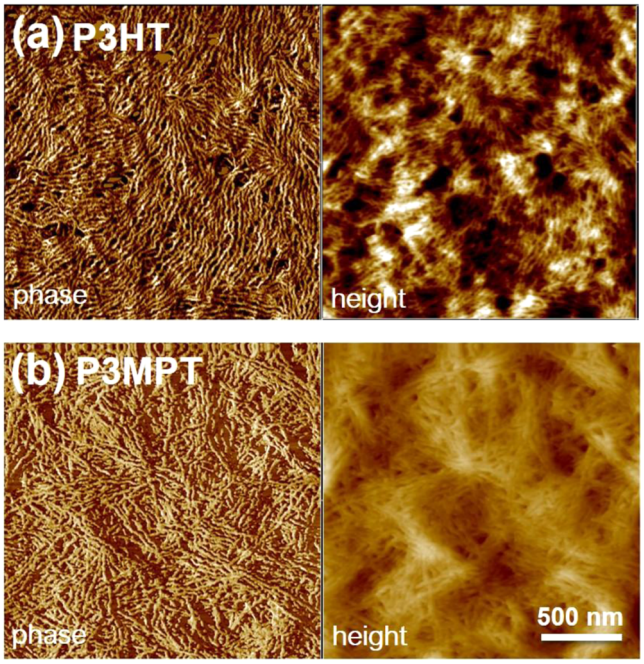


**Figure 3.** AFM images of (a) P3HT and (b) P3MPT films.

the amorphous phase,[48] while P3HT exhibits two extra bands at 547 nm (intrachain absorption) and 601 nm (interchain $\pi-\pi$ stacking) from the crystalline phase, in addition to the band of the amorphous phase at 521 nm. This indicates that the packing of P3MPT is not as regular as that of P3HT in the as-cast films and also that the crystallization rate of P3MPT is slower than that of P3HT, consistent with the DSC and GIWAXS results. The absorption spectra of the films annealed at 90 °C for 10 min are compared to those of the as-cast films in Figure S11. The absorption band of the P3HT film is nearly unchanged after annealing, implying that P3HT can rapidly crystallize during the casting process. In contrast, after annealing, the P3MPT film shows humps at around 550 and 660 nm resulting from the crystalline phase that is absent in the as-cast film. Furthermore, the primary band red-shifts from 506 to 510 nm. These results again evidence that P3MPT diffuses slower than P3HT does and thus requires more time to form crystals.

The normalized UV−vis absorption spectra of P3HT and P3MPT blended with PCBM at a ratio of 1:1 in films are compared with those of the pure polymer films in Figure 4b. Both the bands of P3HT and P3MPT corresponding to the intrachain absorption of the less-ordered chains in the amorphous region blue-shift after mixing with PCBM, from 521 to 515 nm for P3HT and from 506 to 498 nm for P3MPT, respectively.[48] This implies that PCBM can mix well in both the amorphous P3HT and P3MPT, thus reducing the intrachain order.[49] The absorption band at around 333 nm is caused by PCBM, and the absorption intensity of PCBM mixed with P3MPT is much stronger than that mixed with P3HT. It has been shown that the PCBM absorption intensity weakens as the PCBM crystallinity increases.[25,50] In other words, PCBM is less likely to aggregate and form crystals in P3MPT. The slower crystallization of P3MPT excludes less PCBM out of P3MPT crystals and more PCBM can dissolve in the amorphous P3MPT phase, thus alleviating the aggregation of PCBM.[51] These results show that the P3MPT/PCBM blend includes a higher fraction of the molecularly intermixed


https://doi.org/10.1021/acs.macromol.1c00346
Macromolecules 2021, 54, 3689−3699

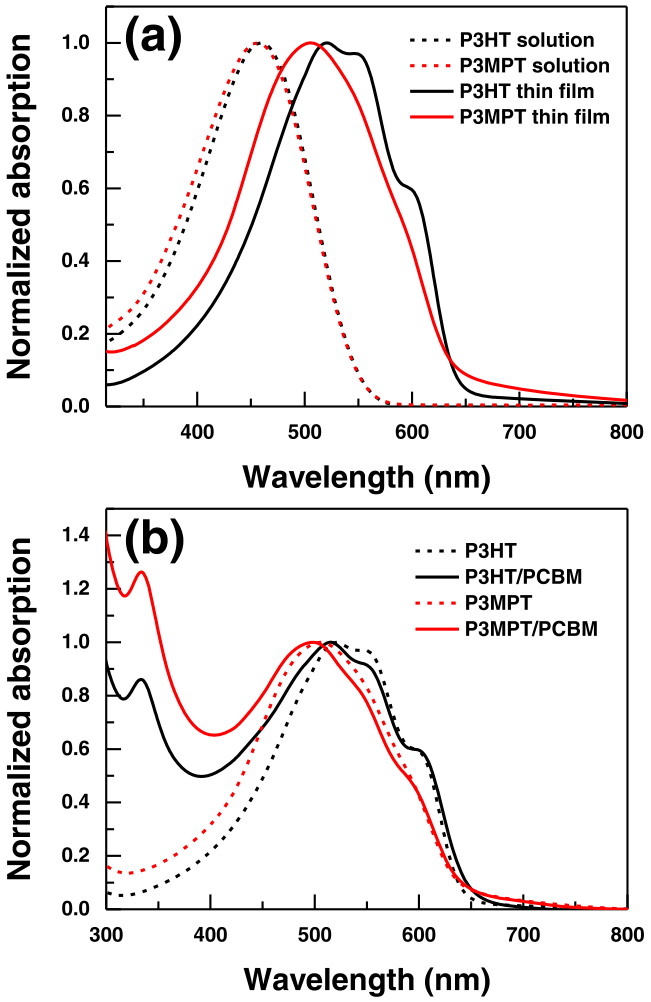


**Figure 4.** Normalized UV−vis absorption spectra of (a) P3HT and P3MPT in solutions and as-cast thin films and (b) P3HT and P3MPT blended with PCBM at the weight ratio of 1:1 in films.

amorphous phase that has been shown to be advantageous to the photovoltaic performance because a more effective charge separation process predominantly occurs in this phase.[25−28]

The PL emissions of pure polymers and their blends with PCBM excited at 500 nm are shown in Figure S12. The emission between 600 and 800 nm greatly weakens when P3HT and P3MPT are blended with PCBM. A high PL quenching allows us to infer that the excitons generated in polymers tend to dissociate at the polymer/PCBM interface rather than recombine in polymers, which evidences that both P3HT and P3MPT can mix well with PCBM in the amorphous phase. The time-resolved photoluminescence (TRPL) spectra of the pure polymers and their blends with PCBM are shown in Figure S13. The samples were excited at 420 nm and then monitored at 650 nm. The PL decay of the pure polymer was fit using the following equation considering a short-lived PL lifetime ($\tau_1$) and a long-lived PL lifetime ($\tau_2$).

$$I(t) = A_1 \exp\left(\frac{-t}{\tau_1}\right) + A_2 \exp\left(\frac{-t}{\tau_2}\right) \quad (6)$$

The short-lived PL lifetime ($\tau_1$) correlates with the trapping of excitons by crystal defects and the long-lived component ($\tau_2$) depends on the crystallinity.[52] The ($\tau_1$, $\tau_2$) of pure P3HT and P3MPT are (84, 383) and (125, 374) ps, respectively, which implies lower crystallinity and fewer crystal defects for pure P3MPT. When blending with PCBM, the decay of the PL emission was fit by the single lifetime equation and the lifetime $\tau$ is greatly decreased, 38 and 37 ps for the P3HT/PCBM and P3MPT/PCBM blends, respectively. This is due to the fast charge separation process at the polymer/PCBM interface, and the P3MPT/PCBM blend shows a marginally higher rate.

Figure 5 shows the data of cyclic voltammetry for P3HT and P3MPT. The oxidation potentials of the polymers were

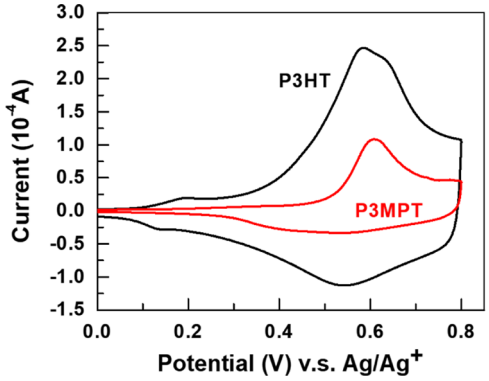


**Figure 5.** Cyclic voltammetry data of P3HT and P3MPT.

measured, and the energy levels of the highest occupied molecular orbital (HOMO) and the lowest unoccupied molecular orbital (LUMO) of the polymers were calculated in combination with the data of UV−vis absorption,[53] as listed in Table 1. The onset oxidation potential $E_{ox}$ of P3MPT (0.52 V) is higher than that of P3HT (0.43 V) because the larger steric hindrance of the branched side chains lowers the conjugation length of P3MPT and thus reduces the electron-donating capability.[11] The energy levels of (HOMO, LUMO) for P3HT and P3MPT are (−5.06, −3.13) and (−5.15, −3.20) eV, respectively. The relative energy levels of the P3HT/PCBM and P3MPT/PCBM active layers, charge transport layers, and electrodes are drawn in Figure S14.

**Table 1. Absorption, Electrochemical Properties, and Energy Levels of P3HT and P3MPT**

| sample | $\lambda_{onset}$[a] (nm) | $E_{opt}$[b] (eV) | $E_{ox}$[c] (V) | HOMO[d] (eV) | LUMO[e] (eV) |
|---|---|---|---|---|---|
| P3HT | 642 | 1.93 | 0.43 | −5.06 | −3.13 |
| P3MPT | 635 | 1.95 | 0.52 | −5.15 | −3.20 |

[a]$\lambda_{onset}$ is the onset wavelength of the UV−vis absorption for films determined from Figure 4a. [b]$E_{opt}$ = 1240/$\lambda_{onset}$. [c]The reference electrode is Ag/Ag$^+$. [d]HOMO = −e($E_{ox}$ − $E_{1/2}$) − 4.80 eV where $E_{1/2}$ = 0.17 V is the half-wave potential of ferrocene standard. [e]LUMO = HOMO + $E_{opt}$.

**Photovoltaic Performance.** The solar cell performances of P3HT and P3MPT blended with PCBM at a 1:1 weight ratio spin-coated from ODCB and TCB solutions are listed in Table 2. The current density ($J$) vs voltage ($V$) curves are shown in Figure S15. The P3HT/PCBM blend exhibits a higher PCE from ODCB than that from TCB. The averaged PCE of the as-cast P3HT/PCBM active layer is 3.61%, and after annealing at 90 °C for 10 min, the PCE increases to 3.86%, comparable to the values previously reported.[6,54] In contrast, the PCEs of the P3MPT/PCBM blend prepared from TCB are much higher than that from ODCB, 4.65 and 4.80%


https://doi.org/10.1021/acs.macromol.1c00346
Macromolecules 2021, 54, 3689−3699

**Table 2. Photovoltaic Performance of P3HT/PCBM and P3MPT/PCBM at a 1:1 Weight Ratio as the Active Layers Fabricated under Different Conditions**

| sample | solvent | annealing (min) | $V_{oc}$ (V) | $J_{sc}$ (mA/cm$^2$) | *FF* (%) | PCE (%) |
|---|---|---|---|---|---|---|
| P3HT/PCBM | ODCB | 0 | 0.63 | 10.30 ± 0.22 | 55.98 ± 1.71 | 3.61 ± 0.06 |
| | ODCB | 10 | 0.64 | 10.45 ± 0.07 | 57.68 ± 0.40 | 3.86 ± 0.02 |
| | TCB | 0 | 0.60 | 9.88 ± 0.01 | 54.21 ± 0.08 | 3.22 ± 0.00 |
| P3MPT/PCBM | ODCB | 0 | 0.80 | 3.36 ± 0.03 | 37.19 ± 0.47 | 1.00 ± 0.02 |
| | TCB | 0 | 0.76 | 9.30 ± 0.01 | 65.83 ± 0.10 | 4.65 ± 0.01 |
| | TCB | 10 | 0.77 | 9.00 ± 0.02 | 69.19 ± 0.13 | 4.80 ± 0.02 |

for the as-cast and annealed devices from TCB, respectively, and only 1.00% from ODCB. Note that the optimized thickness of the P3MPT/PCBM active layer was about 100 nm, as shown in Table S1. The solvent effect can be mainly attributed to the difference of the evaporation rates between ODCB ($T_b$ = 180 °C) and TCB ($T_b$ = 214 °C) that affects the crystallinity of P3HT and P3MPT during the drying process. For P3HT with a higher crystallization rate, the P3HT film cast from TCB is "over" crystallized due to the low evaporation rate of TCB that allows for more time for P3HT to crystallize. This in turn leads to a too large crystallization-induced phase-separated scale between P3HT and PCBM and thus lowers the short-circuit current ($J_{sc}$) and the fill factor (*FF*) that are generally optimized with continuous channels of ∼10 nm in width within active layers for charges to separate and transport.[32] The higher crystallinity also results in a lower open circuit voltage ($V_{oc}$) of the TCB-cast P3HT film because the charge transfer band of P3HT red-shifts as the crystallinity increases.[55] The crystallization rate of P3MPT is rather low and it does not have sufficient time to appropriately crystallize when cast from the more volatile ODCB. The low crystallinity gives rise to a high $V_{oc}$ but very poor $J_{sc}$ and *FF*, and this can be greatly improved by the use of TCB. Therefore, ODCB with a higher evaporation rate and TCB with a lower evaporation rate are suitable for P3HT and P3MPT, respectively, to form a structure effective in the bulk-heterojunction solar cells.

Comparing the optimized conditions, P3MPT significantly outperforms P3HT in power conversion, mainly attributed to the higher $V_{oc}$ and *FF*. $V_{oc}$ is proportional to the gap between the LUMO of the acceptor and the HOMO of the donor in active layers.[56] As shown in Figure S14 and Table 1, the gap between the LUMO of PCBM and the HOMO of P3MPT is larger than that between PCBM and P3HT, which explains the higher $V_{oc}$ of the P3MPT/PCBM blend. The *FF* value reflects the transfer ability of the charge from the active layer to the electrode.[25,27,57] The nature of P3MPT, including the crystallization rate and the compatibility with PCBM, happens to create a phase-separated structure of intermixed amorphous phase and continuous fine crystalline channels more effective to generate free charges and provide low-resistant pathways for charges to transport, thus leading to a higher *FF* value than that of P3HT. In contrast to $V_{oc}$ and *FF*, the $J_{sc}$ value of the P3MPT/PCBM blend is lower than that of the P3HT/PCBM one. Although an optimized phase-separated structure can enhance $J_{sc}$, another key factor to influence $J_{sc}$ is the light-harvesting efficiency.[58] Because of the lower crystallinity of P3MPT in the cast film, the UV−vis absorption of P3MPT at a higher wavelength (>500 nm) is weaker than that of P3HT, as shown in Figure 4. This may be responsible for the lower $J_{sc}$ of the P3MPT/PCBM blend. The EQE data of the P3HT/PCBM and P3MPT/PCBM blends are shown in Figure S16, which agree with the higher $J_{sc}$ of the P3HT/PCBM blend than that of the P3MPT/PCBM blend from the *IV* measurements.

The dependences of $J_{sc}$ and $V_{oc}$ on light intensity are shown in Figure 6. The slopes of $J_{sc}$ vs light intensity in the log−log

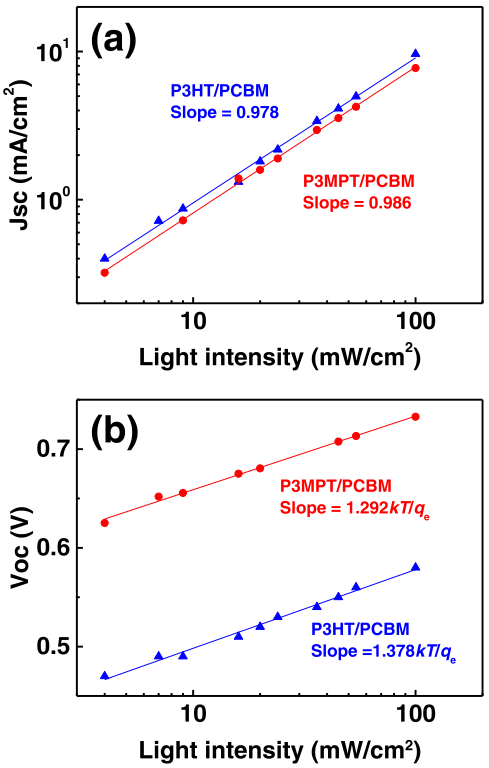


**Figure 6.** Dependence of (a) $J_{sc}$ and (b) $V_{oc}$ on light intensity for the P3HT/PCBM and P3MPT/PCBM blends.

plot for the P3HT/PCBM and P3MPT/PCBM blends are 0.978 and 0.986, respectively. A slope close to 1 indicates that the charge collection efficiency is nearly independent of light intensity and almost all of the excited charges are transferred into electrodes before recombination with a small space charge effect.[59] The dependence of $V_{oc}$ on the logarithm of light intensity gives a slope of $nkTq_e^{-1}$, where $k$ and $q_e$ are the Boltzmann constant and elementary charge, respectively. The $n$ values are 1.378 and 1.292 for the P3HT/PCBM and P3MPT/PCBM blends, respectively. The $n$ value closer to 1 for the P3MPT/PCBM blend implies that it forms a structure with less trap-assisted recombination,[60] which contributes to its higher *FF*.[61] The electron mobility and the hole mobility ($\mu_e$, $\mu_h$) of the P3HT/PCBM and P3MPT/PCBM blends estimated by the SCLC measurements are ($1.61 \times 10^{-3}$, $2.66 \times 10^{-3}$) and ($3.21 \times 10^{-3}$, $6.59 \times 10^{-3}$) cm$^2$/(V s), respectively, as detailed in Figures S17 and S18.[62] The higher


https://doi.org/10.1021/acs.macromol.1c00346
Macromolecules 2021, 54, 3689−3699

*FF* of the P3MPT/PCBM blend also correlates with its higher carrier mobilities.[63]

**Long-Term Stability.** The long-term stability of the P3MPT/PCBM and P3HT/PCBM solar cells fabricated from optimized conditions without annealing was examined. The devices were stored in the dark in a glovebox to prevent light and oxygen, and the dependence of the photovoltaic performance on time was recorded, as shown in Figure 7. The

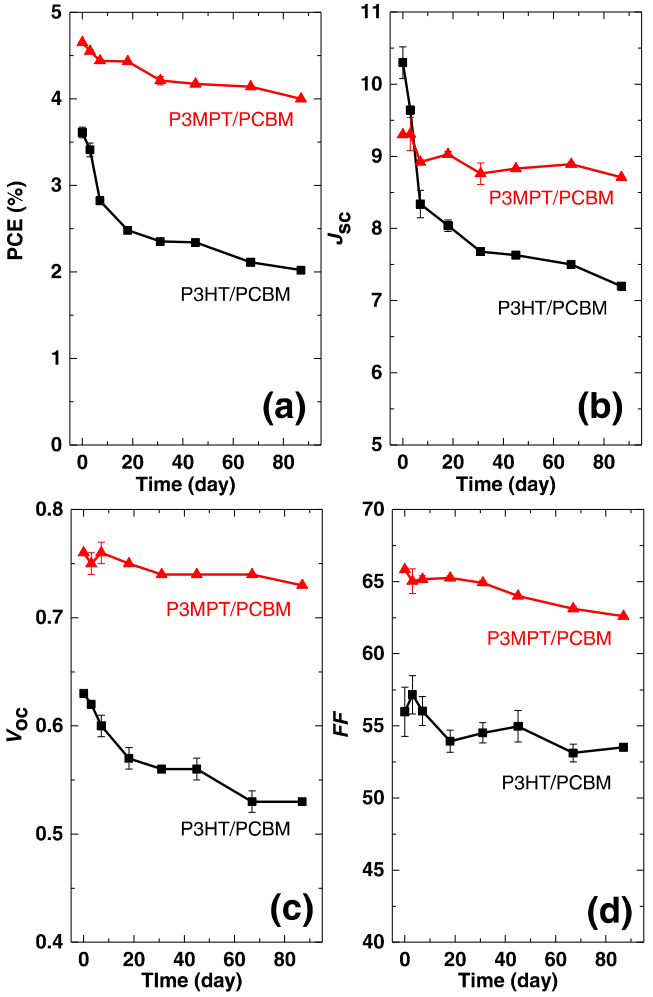


**Figure 7.** Dependence of the solar cell performance on time for the P3HT/PCBM and P3MPT/PCBM blends at a 1:1 weight ratio as active layers: (a) PCE, (b) $J_{sc}$, (c) $V_{oc}$, and (d) *FF*.

PCE of the P3HT/PCBM system greatly decreases from 3.61 to 2.02% (44.0% drop) whereas that of the P3MPT/PCBM system decreases with a much slower rate, from 4.65 to 4.00% (14.0% drop), after 87 days. P3MPT is much more stable than P3HT in photovoltaic performance. The great decrease in the PCE of the P3HT/PCBM system with time mainly results from the severe decay of $J_{sc}$. As shown in Figure 7b, the $J_{sc}$ value of the P3HT/PCBM system rapidly decays from 10.30 to 7.20 mA/cm$^2$ after 87 days, compared to a much slower decay of the P3MPT/PCBM system from 9.30 to 8.71 mA/cm$^2$ after the same time. In Figure 7c, the $V_{oc}$ of the P3MPT/PCBM system is nearly unchanged with time, between 0.76 and 0.73 V, and that of the P3HT/PCBM system decreases from 0.63 to 0.53 V, which also causes the more rapid decay of the P3HT/PCBM cells. The decay rates of the *FF* are similar for both systems, as shown in Figure 7d.

Since the devices were nearly unexposed to light and oxygen that may cause chemical changes to deteriorate the photovoltaic performance,[64] the degradation of the devices should mainly originate from the evolution of the structure in the active layers. We then used the GISAXS technique to probe the structural change with time in the blend thin films. The in-plane ($q_{xy}$) profiles are shown in Figure 8. For all of the

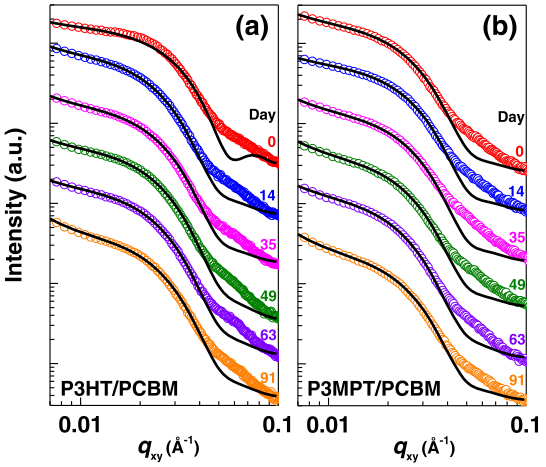


**Figure 8.** GISAXS profiles of (a) P3HT/PCBM and (b) P3MPT/PCBM blends at a 1:1 weight ratio taken at varying times. Model fits are shown as the solid curves through the data.

profiles, scattering shoulders can be seen in the range of $q$ = 0.02−0.04 Å$^{-1}$, which is ascribed to the scattering form factor of P3HT or P3MPT crystallites.[32,41,65] The $q$ ranges of the shoulders are not changed with time for both P3HT and P3MPT in the blends, indicating that the crystallites do not grow at room temperature. The low-$q$ scattering (<0.02 Å$^{-1}$) is contributed from the large scatterers, and in the present cases, the change of intensity in the low-$q$ range should be correlated with the phase-separated scale, specifically, the size of the clusters formed by the polymer crystallites. Larger phase-separation scales lead to a higher slope of the scattering curves at low $q$. For the P3HT/PCBM blend, the slope at low $q$ becomes noticeably steeper after 14 days and then keeps increasing thereafter, while for the P3MPT/PCBM blend, the slope at low $q$ only slightly increases even after 91 days. This indicates that the phase-separated structure of the P3MPT/PCBM blend is more stable than that of the P3HT/PCBM blend with time.

To quantify the structural scales in the blends, we fit the GISAXS profiles combining the model of polydisperse spherical particles to estimate the size of the polymer crystallites and the Debye−Anderson−Brumberger (DAB) model to estimate the phase-separated scales as described in the Experimental Section. The fits are shown in Figure 8 as solid lines through the data, and the fitting parameters are listed in Table 3. In both P3HT and P3MPT blend films, the average radii $R$ of the polymer crystallites are 7−8 nm, close to the reported size of the P3HT crystallites,[41] and the crystallites remain the same size after 91 days. In contrast to the nearly unchanged dimension of crystallites, the correlation length $\xi$, which is proportional to the scale of phase-separation domains, gradually increases with time, especially for the P3HT/PCBM


https://doi.org/10.1021/acs.macromol.1c00346
Macromolecules 2021, 54, 3689−3699

**Table 3. Fitting Parameters from GISAXS Modeling for the P3HT/PCBM and P3MPT/PCBM Systems Changed with Time**

| | P3HT/PCBM | | | P3MPT/PCBM | | |
|---|---|---|---|---|---|---|
| time (day) | $\xi$ (nm) | $R$ (nm) | $p$ | $\xi$ (nm) | $R$ (nm) | $p$ |
| 0 | 31.5 | 7.4 | 0.08 | 31.1 | 7.4 | 0.20 |
| 14 | 44.4 | 7.9 | 0.20 | 30.7 | 7.5 | 0.19 |
| 35 | 45.7 | 7.7 | 0.20 | 32.1 | 7.6 | 0.19 |
| 49 | 47.7 | 7.5 | 0.22 | 32.3 | 7.7 | 0.20 |
| 63 | 48.1 | 7.6 | 0.22 | 33.2 | 7.9 | 0.22 |
| 91 | 48.6 | 7.5 | 0.22 | 34.7 | 7.8 | 0.20 |

blend where $\xi$ greatly increases to 44.4 nm from 31.5 nm after 14 days and then continuously grows to 48.6 nm after 91 days. In the P3MPT/PCBM blend, $\xi$ increases much slowly, from 31.1 nm to 34.7 nm, after the same period of time. The results evidence the stable phase-separated structures of the P3MPT/PCBM blend, consistent with the long-term stability of the photovoltaic performance.

The stability of the phase-separated structures is closely related to the chain mobility and crystallization capability. Theoretically, polymer chains in the amorphous phase are frozen below $T_g$. However, it is known that the measured $T_g$ is a kinetical one and not the real equilibrium $T_g$ that is generally ~50 °C below the measured $T_g$.[66] Therefore, at room temperature (25−30 °C), the polymer chains are not completely frozen and the chain segments in the amorphous phase remain mobile, able to rearrange locally and slowly. The $T_g$ of P3MPT is about 10 °C higher than that of P3HT due to the methyl-branched side chains that retarded the chain mobility, as shown in Figure 2. In other words, P3MPT chains move at a lower rate than P3HT does near room temperature. Therefore, while the P3HT chains keep diffusing to reorganize with time, the P3MPT chains are relatively less mobile under storage. As time increases, the P3HT crystallites cluster slowly to form P3HT-rich domains where the fraction of PCBM dissolved in the amorphous region reduces (Figure 9), which is unfavorable for excited electrons to transport. The $J_{sc}$ thus decays rapidly with time. In contrast, the P3MPT/PCBM blend can maintain its optimal phase-separated structure, which reflects from the nearly constant $V_{oc}$ and the slow decay of the $J_{sc}$, as well as the superior long-term stability of the PCE.

## CONCLUSIONS

Instead of the widely used P3HT that bears linear side chains, in this work, we systematically studied the physical properties and photovoltaic performance of its counterpart with methyl-branched side chains, P3MPT. The methyl group on the side chains provides a higher steric hindrance for the neighbor C−C bond rotation, which causes a more rigid side chain and slower chain mobility, thus leading to a higher glass transition temperature. In addition, the crystallization rate of P3MPT is lower than that of P3HT due to the slower chain diffusion and the bulkier methyl-branched side chain that hinders the chain packing. The lower crystallization rate of P3MPT happens to result in an optimal bulk-heterojunction structure for the power conversion and contribute to the superior long-term stability of the P3MPT/PCBM solar cells. The findings of this work suggest that to achieve stable high-performance polymer solar cells, first, the polymer should crystallize appropriately to form a crystallization-induced phase-separated structure between the donor polymer and the acceptor that can serve as smooth pathways for charges to transport but are fine enough to prevent the recombination of charges. Second, the chain mobility of the polymer should be low, i.e., a higher $T_g$, which can retard the evolution of the optimal bulk-heterojunction structure toward an over-phase-separated scale with time and thus increase the long-term stability. The incorporation of methyl-branched side chains is an effective strategy to simultaneously enhance the power conversion efficiency and the long-term stability of the polythiophene-based solar cells.

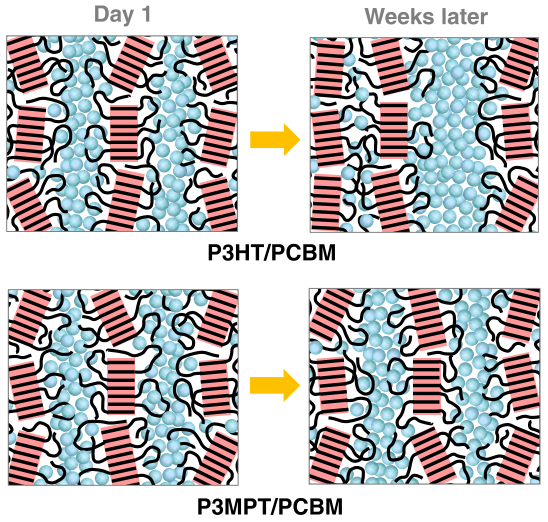


**Figure 9.** Schematics of the active layer morphology on day 1 and after long-time storage for the P3HT/PCBM and P3MPT/PCBM blends. The P3HT crystallite clusters slowly with time to expel PCBM out of the amorphous region between the crystallites while the P3MPT/PCBM blend remains nearly intact due to slow molecular motion.

## ASSOCIATED CONTENT

### Supporting Information

The Supporting Information is available free of charge at https://pubs.acs.org/doi/10.1021/acs.macromol.1c00346.

Synthesis details and characterization of P3MPT; additional DSC, AFM, GISAXS, UV−vis, PL, and EQE data; and energy levels, $J$−$V$ curves, and SCLC modeling of the devices (PDF)

## AUTHOR INFORMATION

### Corresponding Author

**Shih-Huang Tung** − *Institute of Polymer Science and Engineering and Advanced Research Center for Green Materials Science and Technology, National Taiwan University, Taipei 10617, Taiwan;* orcid.org/0000-0002-6787-4955; Email: shtung@ntu.edu.tw

### Authors

**Jia-Yi Chu** − *Institute of Polymer Science and Engineering and Advanced Research Center for Green Materials Science and Technology, National Taiwan University, Taipei 10617, Taiwan*

**Chia-Yi Lin** − *Institute of Polymer Science and Engineering and Advanced Research Center for Green Materials Science and Technology, National Taiwan University, Taipei 10617, Taiwan*



https://doi.org/10.1021/acs.macromol.1c00346
Macromolecules 2021, 54, 3689−3699

**Tsung-Han Tu** − *Department of Chemistry, National Taiwan University, Taipei 10617, Taiwan*
**Shao-Huan Hong** − *Department of Chemical and Materials Engineering, National Central University, Taoyuan 32001, Taiwan*
**Ya-Ying Chang** − *Institute of Polymer Science and Engineering and Advanced Research Center for Green Materials Science and Technology, National Taiwan University, Taipei 10617, Taiwan*
**Chia-Wei Yang** − *Department of Chemistry, National Taiwan University, Taipei 10617, Taiwan*
**Yi-Tsu Chan** − *Department of Chemistry, National Taiwan University, Taipei 10617, Taiwan;* orcid.org/0000-0001-9658-2188
**Cheng-Liang Liu** − *Department of Materials Science and Engineering, National Taiwan University, Taipei 10617, Taiwan;* orcid.org/0000-0002-8778-5386
**Pavel V. Komarov** − *Tver State University, Tver 170100, Russia; A.N. Nesmeyanov Institute of Organoelement Compounds RAS, Moscow 119991, Russia;* orcid.org/0000-0003-2138-5088

Complete contact information is available at: https://pubs.acs.org/10.1021/acs.macromol.1c00346

### Notes

The authors declare no competing financial interest.

## ■ ACKNOWLEDGMENTS

This work was financially supported in part by the "Advanced Research Center of Green Materials Science and Technology" from the Featured Area Research Center Program within the framework of the Higher Education Sprout Project and in part by S.-H.T's research fundings, both of which are granted by the Ministry of Education (109L9006 and 109L893402) and the Ministry of Science and Technology in Taiwan (MOST 106-2628-E-002-006-MY3, 109-2634-F-002-042, and 108-2923-E-002-001-MY3). P.V.K. acknowledges the financial support from the Russian Foundation for Basic Research (19-53-52004). The authors thank National Synchrotron Radiation Research Center, Taiwan, for facilitating the X-ray scattering experiments and Mr. Zong-Ying Liu for assisting in PL measurements.

## ■ REFERENCES

(1) Agbolaghi, S.; Zenoozi, S. A Comprehensive Review on Poly(3-alkylthiophene)-Based Crystalline Structures, Protocols and Electronic Applications. *Org. Electron.* **2017**, *51*, 362−403.
(2) Xin, H.; Kim, F. S.; Jenekhe, S. A. Highly Efficient Solar Cells Based on Poly(3-butylthiophene) Nanowires. *J. Am. Chem. Soc.* **2008**, *130*, 5424−5425.
(3) Samitsu, S.; Shimomura, T.; Heike, S.; Hashizume, T.; Ito, K. Effective Production of Poly(3-alkylthiophene) Nanofibers by Means of Whisker Method Using Anisole Solvent: Structural, Optical, and Electrical Properties. *Macromolecules* **2008**, *41*, 8000−8010.
(4) Sun, Y. P.; Cui, C. H.; Wang, H. Q.; Li, Y. F. High-Efficiency Polymer Solar Cells Based on Poly(3-pentylthiophene) with Indene-C70 Bisadduct as an Acceptor. *Adv. Energy Mater.* **2012**, *2*, 966−969.
(5) Berger, P. R.; Kim, M. Polymer Solar Cells: P3HT: PCBM and beyond. *J. Renewable Sustainable Energy* **2018**, *10*, No. 013508.
(6) Dang, M. T.; Hirsch, L.; Wantz, G. P3HT:PCBM, Best Seller in Polymer Photovoltaic Research. *Adv. Mater.* **2011**, *23*, 3597−3602.
(7) Arosio, P.; Famulari, A.; Catellani, M.; Luzzati, S.; Torsi, L.; Meille, S. V. First Detailed Determination of the Molecular Conformation and the Crystalline Packing of a Chiral Poly(3-alkylthiophene): Poly-3-(S)-2-methylbutylthiophene. *Macromolecules* **2007**, *40*, 3−5.
(8) Catellani, M.; Luzzati, S.; Bertini, F.; Bolognesi, A.; Lebon, F.; Longhi, G.; Abbate, S.; Famulari, A.; Meille, S. V. Solid-State Optical and Structural Modifications Induced by Temperature in a Chiral Poly-3-alkylthiophene. *Chem. Mater.* **2002**, *14*, 4819−4826.
(9) Langeveld-Voss, B. M. W.; Christiaans, M. P. T.; Janssen, R. A. J.; Meijer, E. W. Inversion of Optical Activity of Chiral Polythiophene Aggregates by a Change of Solvent. *Macromolecules* **1998**, *31*, 6702−6704.
(10) Hollamby, M. J.; Nakanishi, T. The Power of Branched Chains: Optimising Functional Molecular Materials. *J. Mater. Chem. C* **2013**, *1*, 6178−6183.
(11) Cui, C. H.; Sun, Y. P.; Zhang, Z. G.; Zhang, M. J.; Zhang, J.; Li, Y. F. Effect of Branched Side Chains on the Physicochemical and Photovoltaic Properties of Poly(3-hexylthiophene) Isomers. *Macromol. Chem. Phys.* **2012**, *213*, 2267−2274.
(12) Chen, H. C.; Wu, I. C.; Hung, J. H.; Chen, F. J.; Chen, I. W. P.; Peng, Y. K.; Lin, C. S.; Chen, C. H.; Sheng, Y. J.; Tsao, H. K.; Chou, P. T. Superiority of Branched Side Chains in Spontaneous Nanowire Formation: Exemplified by Poly(3-2-methylbutylthiophene) for High-Performance Solar Cells. *Small* **2011**, *7*, 1098−1107.
(13) Thompson, B. C.; Frechet, J. M. J. Organic Photovoltaics - Polymer-Fullerene Composite Solar Cells. *Angew. Chem., Int. Ed.* **2008**, *47*, 58−77.
(14) Yu, G.; Gao, J.; Hummelen, J. C.; Wudl, F.; Heeger, A. J. Polymer Photovoltaic Cells: Enhanced Efficiencies via a Network of Internal Donor-Acceptor Heterojunctions. *Science* **1995**, *270*, 1789−1791.
(15) Yao, H. F.; Wang, J. W.; Xu, Y.; Zhang, S. Q.; Hou, J. H. Recent Progress in Chlorinated Organic Photovoltaic Materials. *Acc. Chem. Res.* **2020**, *53*, 822−832.
(16) Shaw, P. E.; Ruseckas, A.; Samuel, I. D. W. Exciton Diffusion Measurements in Poly(3-hexylthiophene). *Adv. Mater.* **2008**, *20*, 3516−3520.
(17) Liu, F.; Gu, Y.; Jung, J. W.; Jo, W. H.; Russell, T. P. On the Morphology of Polymer-Based Photovoltaics. *J. Polym. Sci., Part B: Polym. Phys.* **2012**, *50*, 1018−1044.
(18) Kim, Y.; Choulis, S. A.; Nelson, J.; Bradley, D. D. C.; Cook, S.; Durrant, J. R. Composition and Annealing Effects in Polythiophene/Fullerene Solar Cells. *J. Mater. Sci.* **2005**, *40*, 1371−1376.
(19) Padinger, F.; Rittberger, R. S.; Sariciftci, N. S. Effects of Postproduction Treatment on Plastic Solar Cells. *Adv. Funct. Mater.* **2003**, *13*, 85−88.
(20) Liu, Y.; Zhao, J.; Li, Z.; Mu, C.; Ma, W.; Hu, H.; Jiang, K.; Lin, H.; Ade, H.; Yan, H. Aggregation and Morphology Control Enables Multiple Cases of High-Efficiency Polymer Solar Cells. *Nat. Commun.* **2014**, *5*, No. 5293.
(21) Cates, N. C.; Gysel, R.; Beiley, Z.; Miller, C. E.; Toney, M. F.; Heeney, M.; McCulloch, I.; McGehee, M. D. Tuning the Properties of Polymer Bulk Heterojunction Solar Cells by Adjusting Fullerene Size to Control Intercalation. *Nano Lett.* **2009**, *9*, 4153−4157.
(22) Jo, J.; Kim, S.-S.; Na, S.-I.; Yu, B.-K.; Kim, D.-Y. Time-Dependent Morphology Evolution by Annealing Processes on Polymer:Fullerene Blend Solar Cells. *Adv. Funct. Mater.* **2009**, *19*, 866−874.
(23) Shin, M.; Kim, H.; Park, J.; Nam, S.; Heo, K.; Ree, M.; Ha, C.-S.; Kim, Y. Abrupt Morphology Change upon Thermal Annealing in Poly(3-Hexylthiophene)/Soluble Fullerene Blend Films for Polymer Solar Cells. *Adv. Funct. Mater.* **2010**, *20*, 748−754.
(24) Bertho, S.; Janssen, G.; Cleij, T. J.; Conings, B.; Moons, W.; Gadisa, A.; D'Haen, J.; Goovaerts, E.; Lutsen, L.; Manca, J.; Vanderzande, D. Effect of Temperature on the Morphological and Photovoltaic Stability of Bulk Heterojunction Polymer: Fullerene Solar Cells. *Sol. Energy Mater. Sol. Cells* **2008**, *92*, 753−760.
(25) Westacott, P.; Tumbleston, J. R.; Shoaee, S.; Fearn, S.; Bannock, J. H.; Gilchrist, J. B.; Heutz, S.; deMello, J.; Heeney, M.; Ade, H.; Durrant, J.; McPhail, D. S.; Stingelin, N. On the Role of

Intermixed Phases in Organic Photovoltaic Blends. *Energy Environ. Sci.* **2013**, *6*, 2756−2764.
(26) Scarongella, M.; Paraecattil, A. A.; Buchaca-Domingo, E.; Douglas, J. D.; Beaupre, S.; McCarthy-Ward, T.; Heeney, M.; Moser, J. E.; Leclerc, M.; Frechet, J. M. J.; Stingelin, N.; Banerji, N. The Influence of Microstructure on Charge Separation Dynamics in Organic Bulk Heterojunction Materials for Solar Cell Applications. *J. Mater. Chem. A* **2014**, *2*, 6218−6230.
(27) Kästner, C.; Rathgeber, S.; Egbe, D. A. M.; Hoppe, H. Improvement of Photovoltaic Performance by Ternary Blending of Amorphous and Semi-Crystalline Polymer Analogues with PCBM. *J. Mater. Chem. A* **2013**, *1*, 3961−3969.
(28) Ma, W.; Kim, J. Y.; Lee, K.; Heeger, A. J. Effect of the Molecular Weight of Poly(3-hexylthiophene) on the Morphology and Performance of Polymer Bulk Heterojunction Solar Cells. *Macromol. Rapid Commun.* **2007**, *28*, 1776−1780.
(29) Hiemenz, P. C.; Lodge, T. P. *Polymer Chemistry*, 2nd ed; CRC Press, 2007.
(30) Shen, M. C.; Eisenberg, A. Glass Transitions in Polymers. *Prog. Solid State Chem.* **1967**, *3*, 407−481.
(31) Ro, H. W.; Akgun, B.; O'Connor, B. T.; Hammond, M.; Kline, R. J.; Snyder, C. R.; Satija, S. K.; Ayzner, A. L.; Toney, M. F.; Soles, C. L.; DeLongchamp, D. M. Poly(3-hexylthiophene) and [6,6]-Phenyl-C61-butyric Acid Methyl Ester Mixing in Organic Solar Cells. *Macromolecules* **2012**, *45*, 6587−6599.
(32) Kohn, P.; Rong, Z.; Scherer, K. H.; Sepe, A.; Sommer, M.; Müller-Buschbaum, P.; Friend, R. H.; Steiner, U.; Hüttner, S. Crystallization-Induced 10-nm Structure Formation in P3HT/PCBM Blends. *Macromolecules* **2013**, *46*, 4002−4013.
(33) Kim, B. J.; Miyamoto, Y.; Ma, B.; Fréchet, J. M. J. Photocrosslinkable Polythiophenes for Efficient, Thermally Stable, Organic Photovoltaics. *Adv. Funct. Mater.* **2009**, *19*, 2273−2281.
(34) Griffini, G.; Douglas, J. D.; Piliego, C.; Holcombe, T. W.; Turri, S.; Fréchet, J. M. J.; Mynar, J. L. Long-Term Thermal Stability of High-Efficiency Polymer Solar Cells Based on Photocrosslinkable Donor-Acceptor Conjugated Polymers. *Adv. Mater.* **2011**, *23*, 1660−1664.
(35) Johnson, B. H.; Allagoa, E.; Thomas, R. L.; Stettler, G.; Wallis, M.; Peel, J. H.; Adalsteinsson, T.; McNelis, B. J.; Barber, R. P., Jr Influence of Functionalized Fullerene Structure on Polymer Photovoltaic Degradation. *Sol. Energy Mater. Sol. Cells* **2010**, *94*, 537−541.
(36) Cheng, Y.-J.; Hsieh, C.-H.; Li, P.-J.; Hsu, C.-S. Morphological Stabilization by In Situ Polymerization of Fullerene Derivatives Leading to Efficient, Thermally Stable Organic Photovoltaics. *Adv. Funct. Mater.* **2011**, *21*, 1723−1732.
(37) Li, Z.; Wong, H. C.; Huang, Z.; Zhong, H.; Tan, C. H.; Tsoi, W. C.; Kim, J. S.; Durrant, J. R.; Cabral, J. T. Performance Enhancement of Fullerene-Based Solar Cells by Light Processing. *Nat. Commun.* **2013**, *4*, No. 2227.
(38) Sary, N.; Richard, F.; Brochon, C.; Leclerc, N.; Lévêque, P.; Audinot, J.-N.; Berson, S.; Heiser, T.; Hadziioannou, G.; Mezzenga, R. A New Supramolecular Route for Using Rod-Coil Block Copolymers in Photovoltaic Applications. *Adv. Mater.* **2010**, *22*, 763−768.
(39) Tsai, J.-H.; Lai, Y.-C.; Higashihara, T.; Lin, C.-J.; Ueda, M.; Chen, W.-C. Enhancement of P3HT/PCBM Photovoltaic Efficiency Using the Surfactant of Triblock Copolymer Containing Poly(3-hexylthiophene) and Poly(4-vinyltriphenylamine) Segments. *Macromolecules* **2010**, *43*, 6085−6091.
(40) Zhou, K.; Xin, J. M.; Ma, W. Hierarchical Morphology Stability under Multiple Stresses in Organic Solar Cells. *ACS Energy Lett.* **2019**, *4*, 447−455.
(41) Liu, C. H.; Tseng, W. H.; Cheng, C. Y.; Wu, C. I.; Chou, P. T.; Tung, S. H. Effects of Amorphous Poly(3-hexylthiophene) on Active-Layer Structure and Solar Cells Performance. *J. Polym. Sci., Part B: Polym. Phys.* **2016**, *54*, 975−985.
(42) Jeng, U.-S.; Su, C. H.; Su, C.-J.; Liao, K.-F.; Chuang, W.-T.; Lai, Y.-H.; Chang, J.-W.; Chen, Y.-J.; Huang, Y.-S.; Lee, M.-T.; Yu, K.-L.; Lin, J.-M.; Liu, D.-G.; Chang, C.-F.; Liu, C.-Y.; Chang, C.-H.; Liang, K. S. A Small/Wide-Angle X-ray Scattering Instrument for Structural Characterization of Air-Liquid Interfaces, Thin Films and Bulk Specimens. *J. Appl. Crystallogr.* **2010**, *43*, 110−121.
(43) Kotlarchyk, M.; Chen, S. H. Analysis of Small Angle Neutron Scattering Spectra from Polydisperse Interacting Colloids. *J. Chem. Phys.* **1983**, *79*, 2461−2469.
(44) Debye, P.; Anderson, H. R.; Brumberger, H. Scattering by an Inhomogeneous Solid. II. The Correlation Function and Its Application. *J. Appl. Phys.* **1957**, *28*, 679−683.
(45) Kline, S. R. Reduction and Analysis of SANS and USANS Data Using IGOR Pro. *J. Appl. Crystallogr.* **2006**, *39*, 895−900.
(46) Schulz, G. V. The kinetics of chain polymerisation V. The influence of various types of reactions on the poly-molecularity. *Z. Phys. Chem. B* **1939**, *43*, 25−46.
(47) Zhao, J.; Swinnen, A.; Van Assche, G.; Manca, J.; Vanderzande, D.; Van Mele, B. Phase Diagram of P3HT/PCBM Blends and Its Implication for the Stability of Morphology. *J. Phys. Chem. B* **2009**, *113*, 1587−1591.
(48) Clark, J.; Chang, J.-F.; Spano, F. C.; Friend, R. H.; Silva, C. Determining Exciton Bandwidth and Film Microstructure in Polythiophene Films Using Linear Absorption Spectroscopy. *Appl. Phys. Lett.* **2009**, *94*, No. 163306.
(49) Woo, C. H.; Thompson, B. C.; Kim, B. J.; Toney, M. F.; Fréchet, J. M. J. The Influence of Poly(3-hexylthiophene) Regioregularity on Fullerene-Composite Solar Cell Performance. *J. Am. Chem. Soc.* **2008**, *130*, 16324−16329.
(50) Zhang, Y.; Yip, H.-L.; Acton, O.; Hau, S. K.; Huang, F.; Jen, A. K. Y. A Simple and Effective Way of Achieving Highly Efficient and Thermally Stable Bulk-Heterojunction Polymer Solar Cells Using Amorphous Fullerene Derivatives as Electron Acceptor. *Chem. Mater.* **2009**, *21*, 2598−2600.
(51) Watts, B.; Belcher, W. J.; Thomsen, L.; Ade, H.; Dastoor, P. C. A Quantitative Study of PCBM Diffusion during Annealing of P3HT:PCBM Blend Films. *Macromolecules* **2009**, *42*, 8392−8397.
(52) Yang, W. S.; Park, B. W.; Jung, E. H.; Jeon, N. J.; Kim, Y. C.; Lee, D. U.; Shin, S. S.; Seo, J.; Kim, E. K.; Noh, J. H.; Seok, S. I. Iodide Management in Formamidinium-Lead-Halide-Based Perovskite Layers for Efficient Solar Cells. *Science* **2017**, *356*, 1376−1379.
(53) Muhammad, F. F.; Sulaiman, K. Tuning the Optical Band Gap of DH6T by Alq3 Dopant. *Sains Malays.* **2011**, *40*, 17−20.
(54) Liu, F.; Chen, D.; Wang, C.; Luo, K. Y.; Gu, W. Y.; Briseno, A. L.; Hsu, J. W. P.; Russell, T. P. Molecular Weight Dependence of the Morphology in P3HT:PCBM Solar Cells. *ACS Appl. Mater. Interfaces* **2014**, *6*, 19876−19887.
(55) Vandewal, K.; Gadisa, A.; Oosterbaan, W. D.; Bertho, S.; Banishoeib, F.; Van Severen, I.; Lutsen, L.; Cleij, T. J.; Vanderzande, D.; Manca, J. V. The Relation between Open-Circuit Voltage and the Onset of Photocurrent Generation by Charge-Transfer Absorption in Polymer: Fullerene Bulk Heterojunction Solar Cells. *Adv. Funct. Mater.* **2008**, *18*, 2064−2070.
(56) Li, Y. F.; Cao, Y.; Gao, J.; Wang, D. L.; Yu, G.; Heeger, A. J. Electrochemical Properties of Luminescent Polymers and Polymer Light-Emitting Electrochemical Cells. *Synth. Met.* **1999**, *99*, 243−248.
(57) Bartelt, J. A.; Beiley, Z. M.; Hoke, E. T.; Mateker, W. R.; Douglas, J. D.; Collins, B. A.; Tumbleston, J. R.; Graham, K. R.; Amassian, A.; Ade, H.; Fréchet, J. M. J.; Toney, M. F.; McGehee, M. D. The Importance of Fullerene Percolation in the Mixed Regions of Polymer−Fullerene Bulk Heterojunction Solar Cells. *Adv. Energy Mater.* **2013**, *3*, 364−374.
(58) Chen, C. M.; Jen, T. H.; Chen, S. A. Effective End Group Modification of Poly(3-hexylthiophene) with Functional Electron-Deficient Moieties for Performance Improvement in Polymer Solar Cell. *ACS Appl. Mater. Interfaces* **2015**, *7*, 20548−20555.
(59) Koster, L. J. A.; Mihailetchi, V. D.; Xie, H.; Blom, P. W. M. Origin of the Light Intensity Dependence of the Short-Circuit Current of Polymer/Fullerene Solar Cells. *Appl. Phys. Lett.* **2005**, *87*, No. 203502.


https://doi.org/10.1021/acs.macromol.1c00346
*Macromolecules* 2021, 54, 3689−3699

(60) Cowan, S. R.; Roy, A.; Heeger, A. J. Recombination in Polymer-Fullerene Bulk Heterojunction Solar Cells. *Phys. Rev. B* **2010**, *82*, No. 245207.
(61) Sergeeva, N.; Ullbrich, S.; Hofacker, A.; Koerner, C.; Leo, K. Structural Defects in Donor-Acceptor Blends: Influence on the Performance of Organic Solar Cells. *Phys. Rev. Appl.* **2018**, *9*, No. 024039.
(62) Kim, S.-K.; Yang, H.; Kim, Y. S. Control of Carrier Injection and Transport in Quantum Dot Light Emitting Diodes (QLEDs) via Modulating Schottky Injection Barrier and Carrier Mobility. *J. Appl. Phys.* **2019**, *126*, No. 185702.
(63) Bartelt, J. A.; Lam, D.; Burke, T. M.; Sweetnam, S. M.; McGehee, M. D. Charge-Carrier Mobility Requirements for Bulk Heterojunction Solar Cells with High Fill Factor and External Quantum Efficiency > 90%. *Adv. Energy Mater.* **2015**, *5*, No. 1500577.
(64) Jørgensen, M.; Norrman, K.; Gevorgyan, S. A.; Tromholt, T.; Andreasen, B.; Krebs, F. C. Stability of Polymer Solar Cells. *Adv. Mater.* **2012**, *24*, 580−612.
(65) Gu, Y.; Wang, C.; Liu, F.; Chen, J.; Dyck, O. E.; Duscher, G.; Russell, T. P. Guided Crystallization of P3HT in Ternary Blend Solar Cell Based on P3HT:PCPDTBT:PCBM. *Energy Environ. Sci.* **2014**, *7*, 3782−3790.
(66) Zhou, D. L.; Zhang, G. G. Z.; Law, D.; Grant, D. J. W.; Schmitt, E. A. Physical Stability of Amorphous Pharmaceuticals: Importance of Configurational Thermodynamic Quantities and Molecular Mobility. *J. Pharm. Sci.* **2002**, *91*, 1863−1872.


https://doi.org/10.1021/acs.macromol.1c00346
*Macromolecules* 2021, 54, 3689−3699